Quantum dynamical study of the H_2 and D_2 dissociative adsorption and diffraction from the NiAl (110) alloy surface

P. Rivière,[1] M. F. Somers,[2] G. J. Kroes,[2] and F. Martín[1]
[1]*Departamento de Química, Facultad de Ciencias C-9, Universidad Autónoma de Madrid, 28049 Madrid, Spain*
[2]*Leiden Institute of Chemistry, Gorlaeus Laboratories, Leiden University, P.O. Box 9502, 2300 RA Leiden, The Netherlands*
(Received 23 February 2006; published 22 May 2006)

We present quantum dynamics calculations of dissociative adsorption and elastic and rotationally inelastic diffraction of H_2 and D_2 molecules from the NiAl (110) alloy surface using a six-dimensional potential energy surface obtained with density functional theory (DFT), employing the PW91 generalized gradient approximation. Good agreement with the existing experimental data for both sticking and diffraction is found, thus showing that the electronically adiabatic, rigid-surface model incorporating motion in all H_2 degrees of freedom accurately describes the H_2/NiAl (110) system with the DFT potential employed. The present results confirm previous classical dynamics predictions such as the variation of the sticking coefficient with incidence energy or the importance of both in-plane and out-of-plane (elastic and rotationally inelastic) diffraction below the dissociation threshold. Nevertheless, quantum interference effects, not represented in classical dynamics calculations, lead to structures in the sticking probability near threshold that are not observed in the classical calculations. In the case of diffraction, very good agreement between theory and experiment has been found for specular, in-plane, and out-of-plane elastic diffraction peaks. In the latter case, quantum dynamics gives a more accurate overall description than classical dynamics, which, however, does a quite reasonable job and predicts the main peaks.

DOI: 10.1103/PhysRevB.73.205417 PACS number(s): 68.43.Bc, 68.43.Pq, 79.20.Rf, 82.65.+r

I. INTRODUCTION

The study of adsorption and scattering of H_2 by metal surfaces is important to understand the microscopic mechanisms behind many catalytic reactions. In recent years, full dimensional dynamical calculations based on potential energy surfaces (PES's) obtained from first-principles calculations have provided unprecedented insight into those mechanisms.[1–13] However, despite the fact that real catalyst surfaces often have more than one component, only a few classical dynamics calculations have been performed on an allow surface so far.[14,15]

Surfaces of ordered alloys are ideal to study some aspects of real catalysts while still preserving the advantages of a well-characterized surface, which is more convenient for a direct comparison with experiments.[16] The NiAl (110) surface is composed of equal quantities of Ni and Al atoms. Surfaces made of pure Ni or pure Al exhibit very different reactivities: while dissociation of H_2 on a Ni surface takes place without or with small activation energy barriers,[6,17] dissociation of H_2 on Al is a highly activated process.[18,19] Therefore, a strong site selectivity can be expected for this system.[14] The NiAl (110) surface exhibits a rippled relaxation, in which Al atoms are expanded toward the vacuum, while Ni atoms are contracted toward the bulk. This feature of the surface raised a lot of interest in the 1980s, leading to several experimental studies.[20–23] Theoretical studies of this rippled relaxation[24] and of the interaction of the surface with atomic[25,26] and molecular[27] hydrogen were also performed using density functional theory (DFT).[28,29] Hammer and Scheffler[27] determined, for selected molecular orientations and positions over the unit cell, activation barriers for dissociative adsorption of 0.5 eV and 1.3 eV on Ni and Al sites, respectively.

In more recent molecular beam experiments, the initial sticking coefficient[30] and the relative intensity of elastic and rotationally inelastic diffraction (RID) peaks[31] have been measured for different incidence conditions (impact energy, angle of incidence, etc.). A realistic computational description of reaction of hydrogen on and diffractive scattering of hydrogen from a metal surface is possible within the Born-Oppenheimer and rigid-surface approximations, provided that all six molecular degrees of freedom of H_2 (6D) are described without approximations.[32,33] The 6D PES of the H_2/NiAl (110) system has recently been obtained by Rivière *et al.*[34] in the framework of DFT. In the latter work, a minimum activation barrier of ~300 meV has been predicted. This value is lower than that previously found by Hammer and Scheffler[27] because, in the latter work, a smaller basis set and a less refined pseudopotential and exchange-correlation functional were used. The PES of Ref. 34 has been used to evaluate H_2 and D_2 sticking[14] and diffraction probabilities[14,35,36] using classical dynamics methods.[14] For both sticking and diffraction, the results are in reasonable agreement with the experiments.[30,31] The role of orientational forces in determining the amount of dissociative adsorption and rotational excitation in H_2/NiAl (110) has also been investigated[15] using classical trajectory methods.

So far, a full dimensional quantum treatment of the dynamics of this system is lacking. In this paper we present quantum dynamics calculations for dissociative adsorption, diffraction, and rotational excitation of H_2 and D_2 impinging on the NiAl (110) surface, at normal and non-normal incidence. Quantum results are compared with classical results and with the available experimental data.

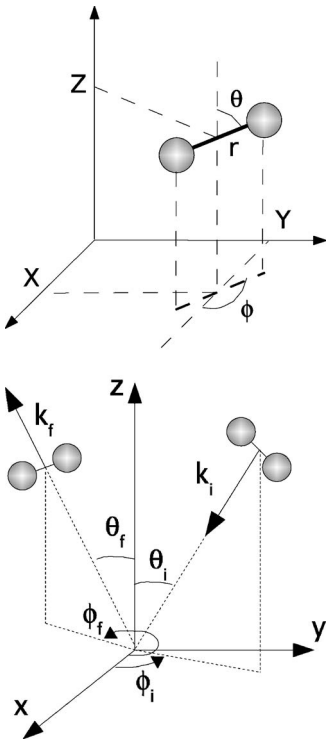

FIG. 1. *Upper*: definition of the six degrees of freedom considered in the dynamics. *Lower*: definition of the coordinates used to define the orientation of the molecular beam.

II. THEORETICAL METHODS

We use a potential energy surface[34] obtained from interpolation of DFT data obtained within the PW91 generalized gradient approximation[37] (GGA) using the corrugation reducing procedure (CRP).[38] The CRP has been shown to provide a precision better than 30 meV in the dynamically relevant regions for several H_2-metal systems.[34,39,40] This error is comparable to what can be expected from DFT calculations themselves. With this PES we have performed 6D quantum calculations (Q), together with classical (C) and quasiclassical (QC) trajectory calculations in which the six diatom degrees of freedom (and not the vibrations of the surface) are included. The six degrees of freedom are the internuclear distance r, the polar (θ) and azimuthal (ϕ) angles associated with the internuclear axis, and the position of the molecular center of mass over the surface (X,Y,Z) (see Fig. 1, left).

Quantum dynamics calculations have been performed using the time-dependent wave packet method (TDWP).[41] In this method the dependence of the wave function on X, Y, Z, and r is represented by a discrete variable representation (DVR).[42] The wave function is transformed from the DVR to a finite basis representation (FBR) through Fast Fourier transforms.[43] Rotations are represented with a non-direct-product FBR, using Gauss-Legendre and Fourier transforms to switch between the FBR and DVR.[44,45] The initial wave function is the product of a Gaussian wave packet in Z and the rovibrational wave function describing the $(J_i,\nu_i=0)$ initial state of the molecule. The time propagation is performed using the split-operator method.[46]

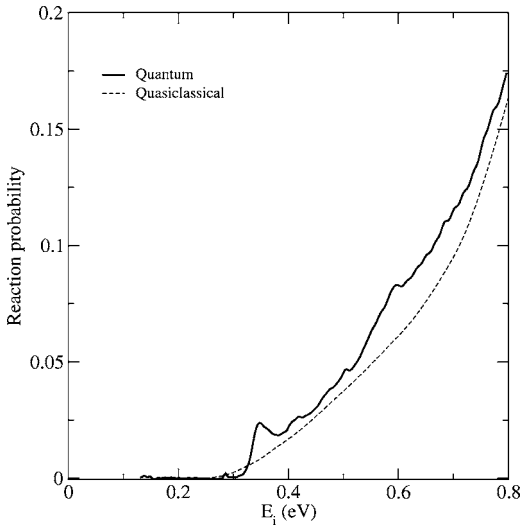

FIG. 2. Sticking coefficient for H_2 $(\nu_i=0,J_i=0)$/NiAl (110) at normal incidence. Solid line: quantum results. Dashed line: quasiclassical results.

The QC calculations take into account the initial vibrational motion of the molecules[47,48] [associated with their vibrational zero-point energy (ZPE)]. This is relevant to describe direct activated adsorption, since classical calculations lead to sticking probabilities significantly lower than the QC and experimental ones (see, e.g., Refs. 4, 7, 39, and 49). However, in QC calculations a vibration to rotation energy transfer can take place, leading to reflected molecules having a vibration energy below the vibrational ZPE, which is forbidden by quantum mechanics. Therefore we have performed QC calculations to study dissociative adsorption, while both C and QC calculations have been performed to study diffraction and rotational excitation probabilities in order to compare their accuracy. In both C and QC calculations, the probability of a given (n,m) diffraction peak has been evaluated as the fraction of trajectories in which the molecule scatters nonreactively with a parallel momentum change contained in the 2D Wigner-Seitz cell built around the (n,m) lattice point in reciprocal space.[36] To determine "quantum" rotational transition probabilities from these classical calculations we have assigned the final rotational quantum number J_f to all trajectories for which $J_f-1\leqslant[-1+\sqrt{1+4|\mathbf{L}_f|^2}]/2\leqslant J_f+1$, where $\mathbf{L}_f$ is the classical angular momentum (see Refs. 10 and 50 and references therein).

Typically, for a given incidence condition, we have run from 20 000 to 50 000 trajectories, depending on the case. The relative statistical error in the calculated probabilities is always less than 1%.

III. DISSOCIATIVE ADSORPTION

In Fig. 2 we show quantum (Q) and quasiclassical (QC) dissociative adsorption probabilities for H_2 $(J_i=0,\ \nu_i=0)$ impinging on NiAl (110) at normal incidence, for an energy range of 0.13–0.8 eV. The quantum calculation has been divided into two parts: one for energies between 0.13 and 0.4 eV and the other for 0.4–0.8 eV. The input parameters for both calculations are shown in Table I.

TABLE I. Parameters used in the quantum calculations for sticking of H_2 ($\nu_i=0$, $J_i=0$) at normal incidence.

Parameter	0.13–0.4 eV	0.4–0.8 eV
Initial wave packet		
Width (a.u.)	1.248	1.158
Z_0 (a.u.)	12.516	same
Normal energy (eV)	0.13–0.4	0.4–0.8
Grid parameters (a.u.)		
Z_i	0.0	same
N_Z	160	same
N_Z^{sp}	240	same
r_i	0.4	same
N_r	40	same
N_X	16	24
N_Y	20	32
ΔZ	0.084	same
Δr	0.2	same
Lattice constants (x,y)	5.465, 7.729	same
Other parameters		
Δt (a.u.)	2.0	same
Propagation time (a.u.)	32 000	25,000
Analysis line (a.u.)	9.492	same
J_{max}	18	same
Z optical potential (a.u.)		
Z_{min}	9.492	same
Proportionality constant A_2	0.005	same
Range in Z	3.864	same
Z^{spec} optical potential (a.u.)		
Z_{min}^{sp}	15.792	same
Proportionality constant A_2	0.005	same
Range in Z	4.284	same
r optical potential (a.u.)		
r_{min}	4.4	same
Proportionality constant A_2	0.005	same
Range in r	3.8	same

The general agreement between the quasiclassical and quantum results is reasonable, although the quasiclassical curve lies below the quantum one for almost all energies. We cannot make a direct comparison between the quantum results and the experiments of Beutl *et al.*[30] because the latter were performed with rotationally hot beams in which the H_2 molecules are in different rovibrational states. However, previously reported quasiclassical results for such hot beams[14] slightly underestimate the experimental sticking probability.[14,30] The reason may be the lack of information about the exact rovibrational distribution of the initial beam, but as the comparison with the quantum results for $J_i=0$ and $\nu_i=0$ shows, it might also be due to a shortcoming of the classical description itself. The quantum dissociation probability exhibits several features that do not appear in the quasiclassical dissociation probability and also not in the experiments:[30] a pronounced peak just above the dissociation threshold and a few less pronounced ones at higher energies. Similar structures have also been observed in quantum dynamics calculations for H_2/Pd (100) (Ref. 1) and H_2/Pd (111) (Refs. 12 and 51), structures that have been attributed to the opening up of new scattering channels—e.g., rotational excitation channels.[52] In our case, the exact origin of the observed structures is not clear since the position of the rotational excitation thresholds does not correspond to that of the observed peaks in Fig. 2 (see also Sec. V). Resonances similar to those reported here have been searched for experimentally,[53,54] but have never been found. A possible explanation is that such peaks are very sensitive to the symmetry of the scattering conditions and, therefore, any surface imperfections such as adatoms or steps would reduce the coherence of the scattering process.[52,55] Furthermore, in a real, experimental situation, the possibility of coupling to phonons and electron-hole pair excitations will ensure that the lifetime associated with resonances is shortened relative to what is found in rigid-surface calculations within the Born-Oppenheimer approximation, so that any features (peaks) found in theoretical calculations should appear much more diffuse (if at all) in experiment.

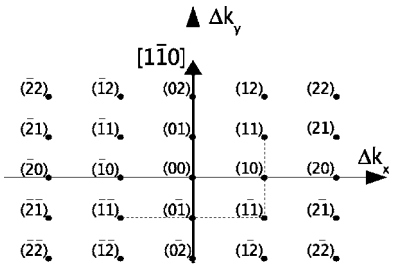

FIG. 3. Reciprocal lattice for the NiAl (110) surface. Numbers within parentheses indicate the corresponding Miller indices. The direction for the diffraction calculations is the [1$\bar{1}$0] indicated in the figure.

IV. DIFFRACTION AND ROTATIONALLY INELASTIC SCATTERING: COMPARISON WITH EXPERIMENT

We have performed quantum calculations for diffraction of H_2 and D_2 from NiAl (110). The reciprocal lattice of NiAl (110) is shown in Fig. 3. There are experimental results for both H_2 and D_2, but since H_2 shows less rotational excitation than D_2, due to the larger energy difference between rotational levels (43 meV in H_2 vs 22 meV in D_2 for the $J=0 \rightarrow 2$ transition), most experiments have made use of D_2.[31] One of the few available H_2 experiments is shown in Fig. 4 for an incidence energy $E_i=74$ meV and an incidence angle of 35° along the [1$\bar{1}$0] direction (see Fig. 3). The diffraction peaks are denoted by their Miller indices (n,m). We have carried out quantum calculations under these incidence conditions using normal hydrogen (i.e., 75% of $J=1$ and 25% of $J=0$) and the input parameters given in Table II. For $J=1$, all values of m_J have been considered. Since the experiment of Ref. 31 does not distinguish between individual m_J quantum numbers and between different values of J_i ($=J_f$) for rotationally elastic diffraction, the probability of the (n,m) dif-

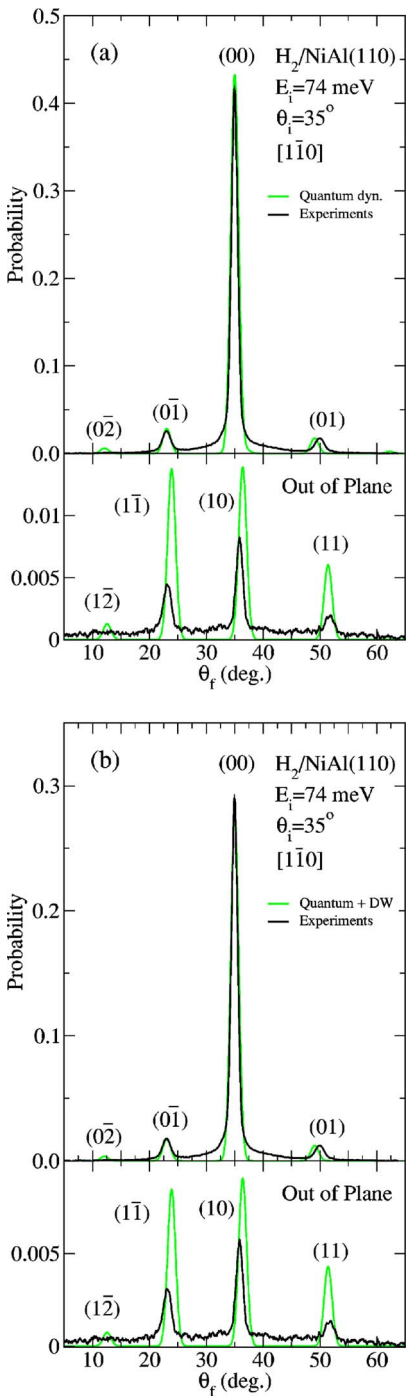

FIG. 4. (Color online) Spectrum for H_2 diffraction on NiAl (110), for E_i=74 meV and θ_i=35°. Solid lines: experimental results from Ref. 31. Dashed lines: quantum-dynamical calculations (see text for details). The top panels correspond to in-plane diffraction, while the lower panels correspond to out-of-plane diffraction. The experimental data are scaled so that the height of the (01) peak is the same as for the theoretical results. In (a) the experimental results are compared with the results from the quantum calculations. In (b) the Debye-Waller correction factor has been applied to the quantum dynamical results (see text for details). Diffraction peaks have been convoluted with a Gaussian function of width 0.7° to account for the limited angular resolution of the experiment.

fraction peak that is directly comparable with experiment can be calculated by first computing

$$\bar{P}^{(n,m)}_{J_i \to J_f} = \frac{1}{2J_i+1} \sum_{m_{J_i}=-J_i}^{J_i} \sum_{m_{J_f}=-J_f}^{J_f} P^{(n,m)}_{J_i,m_{J_i} \to J_f,m_{J_f}}, \tag{1}$$

where $P^{(n,m)}_{J_i,m_{J_i} \to J_f,m_{J_f}}$ is the probability for a specific J_i, $m_{J_i} \to J_f$, m_{J_f} transition, and then taking the appropriate average over J_i (for rotationally elastic diffraction). The results are shown in Fig. 4(a). To obtain a continuous spectrum from the discrete theoretical intensities associated with each diffraction peak we have convoluted to a Gaussian function of 0.7° width. Experimental results have been normalized to the intensity of the (01) peak. The peak heights are converged with a maximum relative error of 1% (2% in the very small out-of-plane peaks).

It can be seen that the agreement between theory and experiment is very good for the in-plane peaks. In the experiment, the (0$\bar{1}$) peak is 16.5 times lower than the specular one, while it is 15.5 times lower in the theory. The (01) peak is 24 times lower in the experiment and 24.5 times lower in the theory. The out-of-plane peaks are almost two orders of magnitude less intense, and this fact is well reproduced by the theory. Obviously, the comparison with experiment for such small probabilities cannot be as good as in the in-plane case, but still the general trends are reasonably reproduced. The comparison is worse for the smallest (1$\bar{1}$) and (11) peaks.

To better judge the quality of the comparison between theory and experiment, one has to analyze the consequences of neglecting the surface temperature in the theoretical calculations. As is well known, both zero-point motion and thermal vibrations of the surface can lead to inelastic scattering of the incoming molecules, which leads to an attenuation of the coherent diffraction intensities and to an increase of the background. This problem, well known in x-ray and neutron diffraction from crystals, is usually taken into account through the so-called Debye-Waller factor (see Ref. 56 and references therein), which relates the intensity $I(T)$ of a diffraction peak with the intensity I_0 which would result from a lattice at rest. The observed intensity is

$$I(T) = I_0 e^{-2W(T)}, \tag{2}$$

where

$$W(T) = \frac{1}{2}\langle (u\Delta k_i)^2 \rangle_T. \tag{3}$$

Here Δk_i is the momentum transfer in the scattering event and u the displacement of a lattice atom from its equilibrium position. This equation implies that diffraction peaks with large momentum transfer will be more attenuated. The Debye-Waller factor for a surface without potential wells can be approximated by (in atomic units) (Refs. 57–59)

$$W(T) = \frac{3(k_{zi} + k_{zf})^2 T}{2M k_B \theta_D^2}, \tag{4}$$

where M is the mass of a surface atom, k_B is the Boltzmann constant, $k_{zi,f}$ is the absolute value of the normal component of the incident and scattered wave vector, and θ_D is the surface Debye temperature. In some cases it is also convenient to use a modified formula that includes the effect of the van der Waals well far from the surface (the Beeby factor[59]). Since the H_2/NiAl (110) PES used in the present work does not exhibit such kind of well,[34] we have preferred to neglect this effect instead of using the well depth as a fitting parameter. In any case, the Debye-Waller factor must be used with caution because it is based on the assumption that the scattering interaction is both weak and short in time, which is not always the case with molecular projectiles.

We have used Eqs. (3) and (4) to estimate the effect of the surface temperature on the diffraction peaks shown in Fig. 4. Both the atomic mass and the Debye surface temperature in Eq. (4) refer to surfaces with a single type of atom. Since NiAl is an alloy with an equal amount of Ni and Al atoms, we have used $W_{\mathrm{NiAl}}(T) = [W_{\mathrm{Ni}}(T) + W_{\mathrm{Al}}(T)]/2$. The surface temperature is 90 K.[31] The Debye surface temperatures are $\theta_D(\mathrm{Ni}) = 375$ K and $\theta_D(\mathrm{Al}) = 394$ K.[60] The resulting corrected spectrum is shown in Fig. 4(b).

It can be seen that the Debye-Waller correction slightly improves the comparison between the experimental data and the theoretical results. The in-plane diffraction spectrum is almost the same as for the rigid surface, although now the specular peak (00) is slightly underestimated instead of being overestimated. Regarding the out-of-plane diffraction spectrum [lower panel in Fig. 4(b)], the intensities of the $(1\bar{1})$ and (10) peaks are now closer to the experimental result. Nevertheless, the Debye-Waller correction is not enough to provide the correct relative intensities of the out-of-plane diffraction peaks. Whether the error in the latter peaks is due to the accuracy of the potential energy surface remains an open question.

We have also studied diffraction of D_2 at higher incidence energies, for which classical dynamics calculations have been found to provide a correct qualitative description of diffraction.[12,14] We have chosen incidence conditions similar to those used in the experiments of Ref. 31: namely, $E_i = 150$ meV, $\theta = 23.5°$ and incidence direction $[1\bar{1}0]$. Under these conditions, the rotational temperature of the incident D_2 beam is ~360 K, which means that rotational levels up to $J_i = 4$ are significantly populated. Consequently, not only diffraction but also rotational excitation and deexcitation is possible. In the quantum dynamics calculations we have limited the number of initial rotational states up to $J_i = 3$; i.e., we have performed 16 different quantum calculations (one per each initial m_{J_i}). The $J_i = 4$ molecules amount to only 12.8% of the incident beam, but imply 9 additional calculations, which is computationally very expensive. The probabilities have been evaluated by weighting the results obtained for each individual rotational level J_i with the corresponding initial populations determined in the experiment.[31] The quantum results are compared in Fig. 5 with the experiment[31] and

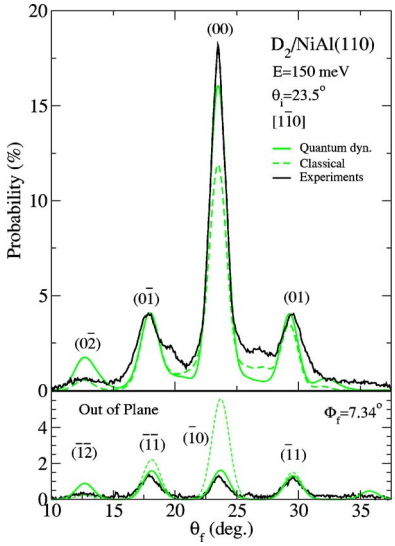

FIG. 5. (Color online) Spectrum for D_2 diffraction on NiAl (110), for $E_i = 150$ meV, $\theta_i = 23.5°$, and an incidence direction $[1\bar{1}0]$. Upper panel: In-plane diffraction. Lower panel: out-of-plane diffraction. Solid black lines: experimental results (Ref. 31). Solid green lines: quantum-dynamical results. Dashed lines: classical results.

the classical results of Ref. 35 for the same incidence conditions. In the figure, Φ_f denotes the experimental reflection angle referred to the incidence plane, related to the angles θ_f and ϕ_f defined in Fig. 1 (left) by $\sin\Phi_f = \sin\theta_f \sin\phi_f$. In the experiments, Φ_f remains constant. The experimental results (in arbitrary units) have been normalized with respect to the (01) peak. It can be seen that the relation between the first order in-plane (IP) peaks (01) and $(0\bar{1})$ and the specular peak is almost the same as in the experiments. However, the specular peak seems to be slightly underestimated. The input parameters are given in Table II. This might be due to the exclusion of molecules with initial $J_i = 4$. Indeed, Table III shows that the contribution of the specular peak (00) increases with J_i, while those of the (01) and $(0\bar{1})$ peaks remain more or less constant. Therefore, inclusion of $J_i = 4$ molecules in the calculations (12.8% of the molecular beam) would increase the size of the specular peak, but not of the (01) and $(0\bar{1})$ peaks. The height of the out-of-plane diffraction peaks is extremely well reproduced by the quantum calculations, especially for the three main peaks. This is in contrast with the classical dynamics results, which overestimate the main out-of-plane diffraction peak $(\bar{1}0)$ by a factor of ~4.

The main rotationally inelastic peaks $0 \rightarrow 2$ and $2 \rightarrow 0$ appear in the region between the specular peak and the (01) or $(0\bar{1})$ peaks (see Fig. 5). While classical calculations predict reasonably well the spectrum in this region, quantum calculations underestimate their intensity. Similar failures of quantum dynamics calculations in describing rotational excitation within the rigid surface approximation have been found in other systems such as H_2/Pd (111) (Ref. 9) and H_2/Pt (111) (Ref. 61) (see also Ref. 32). However, the inclusion of surface vibrations leads, in general, to a much better agreement with experiment.[62,63]

TABLE II. Parameters used in the quantum calculations for diffraction. Numbers within parentheses correspond to ($H_2^{J_i=1}$) and ($D_2^{J_i=1,3}$) and are only given when they differ from those used for $H_2^{J_i=0}$ and $D_2^{J_i=0,2}$, respectively.

Parameter	$H_2^{J_i=0}$ ($H_2^{J_i=1}$)	$D_2^{J_i=0,2}$ ($D_2^{J_i=1,3}$)
Initial wave packet		
Width (a.u.)	0.435094	0.57918
Z_0 (a.u.)	12.5	same
Average energy (eV)	0.078556	0.145711
Grid parameters (a.u.)		
Z_i	0	same
N_Z	90	same
N_Z^{sp}	135	same
r_i	0.4	same
N_r	40 (60)	48
N_X	8	10
N_Y	12	16
ΔZ	0.15	same
Δr	0.2 (0.132)	0.165
Lattice constants (x,y)	5.465, 7.729	same
Other parameters		
Δt (a.u.)	2.5	same
Propagation time (a.u.)	70 000	35 000
Analysis line (a.u.)	9.45	same
J_{max}	8 (9)	8 (9)
Z optical potential (a.u.)		
Z_{min}	9.45	same
A_z	0.003	same
Range in Z	3.9	same
r optical potential (a.u.)		
r_{min}	4.4	4.36
A_r	0.005	same
Range in r	3.8	3.795

Apart from these discrepancies, there is good overall agreement between the classical and quantum results. For instance, the intensity of the $(0\bar{1})$ and (01) peaks is practically the same in both calculations. The largest errors in the classical calculations are for the specular and out-of-plane diffraction peaks. However, classical dynamics calculations correctly predict which are the dominant diffraction peaks and which peaks are not observed even though they are energetically allowed. This is consistent with previous findings in H_2/Pd (111).[12,36] The comparison between classical and quantum dynamics results for rotational excitation deserves a more systematic analysis. This is given in the next section.

V. ROTATIONAL EXCITATION

In order to investigate the role of rotational effects more systematically, we have used the results of the quantum calculations presented in Sec. III (see Table I) to evaluate rotationally inelastic probabilities as functions of incidence energy. In these calculations, the incidence energy varies up to $E_i=0.8$ eV and the H_2 molecule is initially in its ground rovibrational state ($J_i=0$ and $\nu_i=0$).

TABLE III. Probability of the main in-plane peaks for different values of J_i (%), for D_2/NiAl (110), $E_i=150$ meV, and $\theta_i=23.5°$.

Peak	$J_i=0$	$J_i=1$	$J_i=2$	$J_i=3$
(00)	9.038	25.715	33.679	45.353
(01)	10.519	6.390	6.141	7.757
$(0\bar{1})$	9.941	7.193	5.668	8.087

The comparison between classical and quantum rotational excitation probabilities is very good (see Fig. 6), especially at the higher energies. At $E_i\sim0.4$ eV, the agreement between classical and quantum calculations is very good. At lower energies, the classical results overestimate the $0\rightarrow2$ rotational excitation probability. Quasiclassical calculations lead to an even larger overestimation, which is the consequence of the unphysical energy transfer from the ground vibrational state to rotation. In any case, quasiclassical dynamics reproduces qualitatively well the general trend. The differences between classical and quantum calculations may be due to the artificial discretization of the angular momentum. Similar good comparisons between classical and quantum rotational excitation probabilities have been obtained in previous works for other systems, in both low-dimensional models[64] and realistic 6D calculations.[9] An interesting conclusion that can be extracted from Fig. 6 is that excitation to a given rotational level with $J_f>2$ is only effective at energies significantly larger than the $0\rightarrow J_f$ excitation energies, which are 142 meV ($J_f=4$), 293 meV ($J_f=6$), and 493 meV ($J_f=8$).

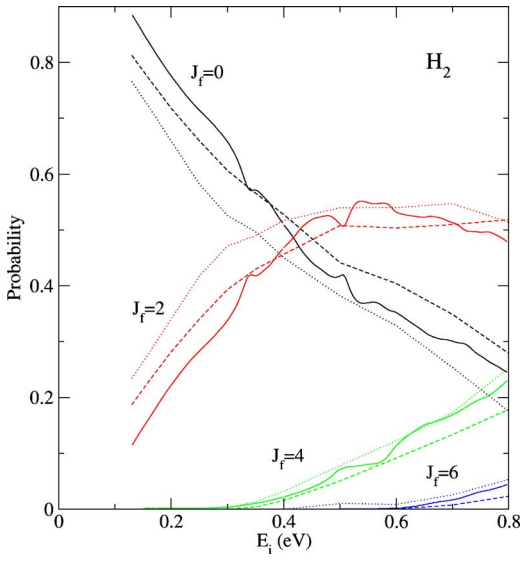

FIG. 6. (Color online) Rotational excitation probabilities as a function of the collision energy for H_2 ($J_i=0$, $\nu_i=0$) impinging on NiAl (110) at normal incidence. Solid lines: quantum calculations (see Table III for details). Dashed lines: classical calculations. Dotted lines: quasiclassical calculations. The rotational excitation probabilities are normalized to the total reflection probability at each energy.

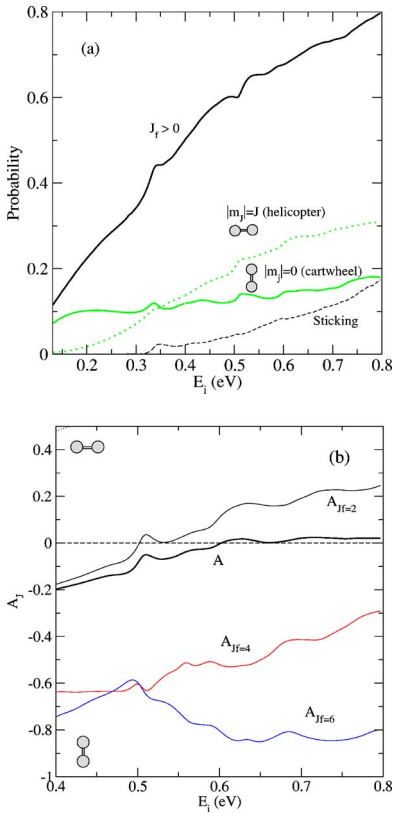

FIG. 7. (a) (Color online) Proportion of rotationally excited ($J_f>0$) cartwheel ($m_{J_f}=0$, solid green line) and helicopter ($|m_{J_f}|=J_f$, dotted green line) molecules relative to the total number of reflected molecules for H_2 ($J_i=0$, $\nu_i=0$) at normal incidence. Solid black line: proportion of rotationally excited molecules relative to the total number of reflected molecules summed over all m_{J_f} values. Dotted black line: absolute sticking probability. (b) Final rotational quadrupole alignment as a function of the incidence energy. Results are shown for $J_f=2,4,6$ and for an average of them (see text for details).

This behavior is different to what has been observed in non-activated systems[1,12,51] and is the reason why it is difficult to understand the origin of the peaks appearing in the sticking probability near the dissociation threshold (see Fig. 2).

As has been discussed in previous works,[15,32] molecules with $|m_{J_i}|=J_i$ (*helicopter* molecules—i.e., molecules that rotate in a plane parallel to the surface) should dissociate more efficiently than molecules with $m_{J_i}=0$ (*cartwheel* molecules—i.e., molecules that rotate in a plane perpendicular to the surface). However, for the $J_i=0$ case considered in this work, one cannot distinguish between these two orientations. Nevertheless, one can investigate the role of orientation effects by looking at the final value of m_{J_f}. Figure 7(a) shows the proportion of rotationally excited ($J_f>0$) cartwheel ($m_{J_f}=0$) and helicopter ($|m_{J_f}|=J_f$) molecules relative to the total number of reflected molecules (hereafter called, for short, *relative* excitation probabilities). For comparison, the relative excitation probability summed over all possible values of m_{J_f} and the absolute sticking probability are also shown. It can be seen that, in agreement with previous classical dynamics predictions on D_2/NiAl (110),[15] the relative probabilities of being rotationally excited in both cartwheel and helicopter configurations increase with incidence energy and that the proportion of rotationally excited helicopter molecules above the dissociation threshold is larger than that of cartwheel molecules. In Ref. 15 it has been shown that, at incidence energies larger than 0.8 eV (i.e., when the sticking probability is larger than 50%), the relative rotational excitation probabilities start decreasing with incidence energy. Such a decrease occurs first for helicopter molecules because these are the molecules with the correct parallel orientation to dissociate on the surface. Molecules that end up dissociating but start their approach to the surface with the wrong orientation must rotate in order to adopt the parallel orientation. Consequently, the fraction of reflected molecules that are rotationally excited decreases as the dissociation probability increases.[15] Although the incidence energies considered in this work are not high enough to clearly observe these effects, Fig. 7(a) shows that the slopes of the corresponding rotational excitation probabilities decrease with incidence energy for $E_i>0.5$ eV, which is in excellent agreement with the classical dynamics predictions of Ref. 15.

A different way to analyze the role of molecular orientation is to look at the rotational quadrupole alignment of reflected molecules defined as

$$A_{J_f}(E,\nu)=\frac{\sum_{m_{J_f}=-J_f}^{J_f}P_{\mathrm{ref}}(J_f,m_{J_f})[3m_{J_f}^2/J_f(J_f+1)-1]}{\sum_{m_{J_f}=-J_f}^{J_f}P_{\mathrm{ref}}(J_f,m_{J_f})}. \tag{5}$$

Its value varies from -1 ($m_{J_f}=0$), which means that only cartwheel molecules are reflected, to a maximum value ($|m_{J_f}|=J_f$), which means that only helicopter molecules are reflected. We have also evaluated an average rotational quadrupole alignment, which takes into account all possible values of $J_f>0$ through the formula

$$A(E,\nu)=\frac{\sum_{J_f\neq 0}\sum_{m_{J_f}=-J_f}^{J_f}P_{\mathrm{ref}}(J_f,m_{J_f})[3m_{J_f}^2/J_f(J_f+1)-1]}{\sum_{J_f\neq 0}\sum_{m_{J_f}=-J_f}^{J_f}P_{\mathrm{ref}}(J_f,m_{J_f})}. \tag{6}$$

The results are shown in Fig. 7(b). It can be seen that $A(E,\nu)$ is close to zero in the whole energy range, meaning that the proportion of helicopter and cartwheel molecules reflected below $E_i=0.8$ eV remains more or less constant. Nevertheless, as for the relative rotational excitation probabilities, there is a change of tendency at around 0.5–0.6 eV, which might also be an indication of the fact that helicopter molecules begin to dissociate earlier than cartwheel molecules. This should lead to a decrease of $A(E,\nu)$ at incidence energies beyond 0.8 eV; however, further research is needed to clear up this particular issue.

VI. CONCLUSION

We have carried out quantum dynamics calculations for dissociative adsorption and diffraction of H_2 and D_2 mol-

ecules from the NiAl (110) surface using a DFT six-dimensional potential energy surface.[34] In particular, we have calculated H_2 ($\nu_i=0$, $J_i=0$) dissociation probabilities for normal incidence and incidence energies $E_i=0.13-0.8$ eV. The results have been compared with those from quasiclassical dynamics calculations. Both calculations lead to a dissociation threshold of around 0.25 eV and to a dissociation probability that increases with incidence energy. These findings are in agreement with the experimental results of Beutl *et al.*[30] The quasiclassical probabilities are slightly lower than the quantum ones in most of the energy range. Also, a narrow peak just above the dissociation threshold and other broader structures at higher energies resulting from quantum interferences are not observed in the quasiclassical calculations.

In-plane and out-of-plane diffraction spectra below the dissociation threshold have been calculated using the same off-normal incidence conditions as in the experiment of Farías *et al.*[31] The calculated relative elastic scattering probabilities are in very good agreement with the experimental ones. There is also a reasonable agreement between quantum and classical results, except for the magnitude of the specular and several out-of-plane diffraction peaks, which are, respectively, underestimated and overestimated in the classical calculations. The comparison between quantum and experimental rotationally inelastic probabilities is worse, but the good agreement between quantum and classical results in a wide range of incidence energies suggests that the reason for the discrepancy with experiment in this particular case might be the use of the rigid-surface approximation. In any case, the quality of the comparison between the quantum dynamics calculations and the existing experimental data for sticking and diffraction shows that the H_2/NiAl (110) potential energy surface recently proposed by Rivière *et al.*[34] is accurate enough to make realistic predictions of sticking and diffraction in this activated system.

ACKNOWLEDGMENTS

This work was partially supported by the DGI (Spain), Project No. CTQ2004-00039/BQU. We thank the CCC-UAM (Spain) for their generous allocation of computer time.

[1] A. Gross, S. Wilke, and M. Scheffler, Phys. Rev. Lett. **75**, 2718 (1995).
[2] G. J. Kroes, E. J. Baerends, and R. C. Mowrey, Phys. Rev. Lett. **78**, 3583 (1997).
[3] A. Gross, Surf. Sci. Rep. **32**, 291 (1998).
[4] D. A. McCormack and G. J. Kroes, Chem. Phys. Lett. **296**, 515 (1998).
[5] D. A. McCormack, G. J. Kroes, R. A. Olsen, E. J. Baerends, and R. C. Mowrey, Phys. Rev. Lett. **82**, 1410 (1999).
[6] G. Kresse, Phys. Rev. B **62**, 8295 (2000).
[7] E. Pijper, M. F. Somers, G. Kroes, R. A. Olsen, E. J. Baerends, H. F. Busnengo, A. Salin, and D. Lemoine, Chem. Phys. Lett. **347**, 277 (2001).
[8] E. Pijper, G. Kroes, R. A. Olsen, and E. J. Baerends, J. Chem. Phys. **117**, 5885 (2002).
[9] H. F. Busnengo, E. Pijper, G. J. Kroes, and A. Salin, J. Chem. Phys. **119**, 12553 (2003).
[10] C. Díaz, H. F. Busnengo, F. Martín, and A. Salin, J. Chem. Phys. **118**, 2886 (2003).
[11] A. Dianat and A. Gross, J. Chem. Phys. **120**, 5339 (2004).
[12] C. Díaz, M. F. Somers, G. J. Kroes, H. F. Busnengo, A. Salin, and F. Martín, Phys. Rev. B **72**, 035401 (2005).
[13] C. Díaz, J. K. Vincent, G. P. Krishnamohan, R. A. Olsen, G. J. Kroes, K. Honkala, and J. K. Nørskov, Phys. Rev. Lett. **96**, 096102 (2006).
[14] P. Rivière, H. F. Busnengo, and F. Martin, J. Chem. Phys. **123**, 074705 (2005).
[15] P. Rivière, A. Salin, and F. Martín, J. Chem. Phys. **124**, 084706 (2006).
[16] B. E. Hayden and A. Hodgson, J. Phys.: Condens. Matter **11**, 8397 (1999).
[17] K. D. Rendulic, G. Anger, and A. Winkler, Surf. Sci. **208**, 404 (1989).
[18] H. F. Berger and K. D. Rendulic, Surf. Sci. **253**, 325 (1991).
[19] B. Hammer, K. W. Jacobsen, and J. K. Nørskov, Phys. Rev. Lett. **69**, 1971 (1992).
[20] H. L. Davis and J. R. Noonan, Phys. Rev. Lett. **54**, 566 (1985).
[21] S. M. Yalisove and W. R. Graham, Surf. Sci. **183**, 556 (1987).
[22] D. R. Mullins and S. H. Overbury, Surf. Sci. **199**, 141 (1988).
[23] S.-C. Lui, M. H. Kang, E. J. Mele, E. W. Plummer, and D. M. Zehner, Phys. Rev. B **39**, 13149 (1989).
[24] J. I. Lee, C. L. Fu, and A. J. Freeman, Phys. Rev. B **36**, R9318 (1987).
[25] A. T. Hanbicki, A. P. Baddorf, E. W. Plummer, B. Hammer, and M. Scheffler, Surf. Sci. **331**, 811 (1995).
[26] M. Konôpka, I. Ŝtich, and K. Terakura, Phys. Rev. B **65**, 125418 (2002).
[27] B. Hammer and M. Scheffler, Phys. Rev. Lett. **74**, 3487 (1995).
[28] P. Hohenberg and W. Kohn, Phys. Rev. **136**, 864 (1964).
[29] W. Kohn and L. J. Sham, Phys. Rev. **140**, 1133 (1965).
[30] M. Beutl, K. D. Rendulic, and G. R. Castro, J. Chem. Soc., Faraday Trans. **91**, 3639 (1995).
[31] D. Farías, R. Miranda, and K. H. Rieder, J. Chem. Phys. **117**, 2255 (2002).
[32] G. J. Kroes and M. F. Somers, J. Theor. Comput. Chem. **4**, 493 (2005).
[33] P. Nieto, E. Pijper, D. Barredo, G. Laurent, R. A. Olsen, E. J. Baerends, G. J. Kroes, and D. Farías, Science **312**, 86 (2006).
[34] P. Rivière, H. F. Busnengo, and F. Martín, J. Chem. Phys. **121**, 751 (2004).
[35] D. Farías, C. Díaz, P. Rivière, H. F. Busnengo, P. Nieto, M. F. Somers, G. J. Kroes, A. Salin, and F. Martín, Phys. Rev. Lett. **93**, 246104 (2004).
[36] C. Díaz, H. F. Busnengo, P. Rivière, D. Farías, P. Nieto, M. F. Somers, G. J. Kroes, A. Salin, and F. Martín, J. Chem. Phys. **122**, 154706 (2005).
[37] J. P. Perdew, J. A. Chevary, S. H. Vosko, K. A. Jackson, M. R. Pederson, D. J. Singh, and C. Fiolhais, Phys. Rev. B **46**, 6671

(1992).
[38] H. F. Busnengo, A. Salin, and W. Dong, J. Chem. Phys. **112**, 7641 (2000).
[39] H. F. Busnengo, C. Crespos, W. Dong, J. C. Rayez, and A. Salin, J. Chem. Phys. **116**, 9005 (2002).
[40] R. Olsen, H. F. Busnengo, A. Salin, M. F. Somers, G. J. Kroes, and E. J. Baerends, J. Chem. Phys. **116**, 3841 (2002).
[41] R. Kosloff, J. Phys. Chem. **92**, 2087 (1988).
[42] J. C. Light, J. P. Hamilton, and J. V. Lill, J. Chem. Phys. **82**, 1400 (1985).
[43] D. Kosloff and R. Kosloff, J. Comput. Phys. **52**, 35 (1983).
[44] G. C. Corey and D. Lemoine, J. Chem. Phys. **97**, 4115 (1992).
[45] D. Lemoine, J. Chem. Phys. **101**, 10526 (1994).
[46] M. D. Feit, J. A. F. Fleck, Jr., and A. Steiger, J. Comput. Phys. **47**, 412 (1982).
[47] M. Karplus, R. N. Porter, and R. D. Sharma, J. Chem. Phys. **43**, 3259 (1965).
[48] R. N. Porter and L. M. Raff, *Dynamics of Molecular Collisions* (Plenum, New York, 1976), Pt. B.
[49] H. F. Busnengo, W. Dong, and A. Salin, Chem. Phys. Lett. **320**, 328 (2000).
[50] C. Díaz, F. Martín, H. F. Busnengo, and A. Salin, J. Chem. Phys. **120**, 321 (2004).
[51] H. F. Busnengo, E. Pijper, M. F. Somers, G. J. Kroes, A. Salin, R. A. Olsen, D. Lemoine, and W. Dong, Chem. Phys. Lett. **356**, 515 (2002).
[52] A. Gross and M. Scheffler, Phys. Rev. Lett. **77**, 405 (1996).
[53] C. T. Rettner and D. J. Auerbach, Chem. Phys. Lett. **253**, 236 (1996).
[54] C. T. Rettner and D. J. Auerbach, Phys. Rev. Lett. **77**, 404 (1996).
[55] A. Gross and M. Scheffler, Chem. Phys. Lett. **256**, 417 (1996).
[56] D. Farías and K. H. Rieder, Rep. Prog. Phys. **61**, 1575 (1998).
[57] J. R. Manson, *Helium Atom Scattering from Surfaces* (Springer-Verlag, Berlin, 1992).
[58] B. Gumhalter, Phys. Rep. **351**, 1 (2001).
[59] J. L. Beeby, J. Phys. C **4**, L359 (1971).
[60] N. W. Ashcroft and N. D. Mermin, *Solid State Physics* (Saunders College, Philadelphia, 1976).
[61] S. M. Kingma, M. F. Somers, E. Pijper, G. J. Kroes, R. A. Olsen, and E. J. Baerends, J. Chem. Phys. **118**, 4190 (2003).
[62] H. F. Busnengo, W. Dong, P. Sautet, and A. Salin, Phys. Rev. Lett. **87**, 127601 (2001).
[63] Z. S. Wang, G. R. Darling, and S. Holloway, J. Chem. Phys. **120**, 2923 (2004).
[64] M. Kay, G. R. Darling, and S. Holloway, J. Chem. Phys. **108**, 4614 (1998).